Theses and Dissertations   1. Thesis and Dissertation Collection, all items

2009-12

Characterization of zinc selenide-based ultraviolet detectors

Naval, Victoriano C.

Monterey, California: Naval Postgraduate School

http://hdl.handle.net/10945/4476

NAVAL
POSTGRADUATE
SCHOOL

MONTEREY, CALIFORNIA

THESIS

**CHARACTERIZATION OF ZINC SELENIDE-BASED
ULTRAVIOLET DETECTORS**

by

Victoriano C. Naval, Jr.

December 2009

Thesis Advisor:	Gamani Karunasiri
Second Reader:	Craig Smith

Approved for public release, distribution is unlimited

THIS PAGE INTENTIONALLY LEFT BLANK

1. AGENCY USE ONLY *(Leave blank)*	2. REPORT DATE December 2009	3. REPORT TYPE AND DATES COVERED Master's Thesis	
4. TITLE AND SUBTITLE Characterization of Zinc Selenide-Based Ultraviolet Detectors		**5. FUNDING NUMBERS**	
6. AUTHOR(S) Victoriano C. Naval, Jr.			
7. PERFORMING ORGANIZATION NAME(S) AND ADDRESS(ES) Naval Postgraduate School Monterey, CA 93943-5000		**8. PERFORMING ORGANIZATION REPORT NUMBER**	
9. SPONSORING /MONITORING AGENCY NAME(S) AND ADDRESS(ES) N/A		**10. SPONSORING/MONITORING AGENCY REPORT NUMBER**	
11. SUPPLEMENTARY NOTES The views expressed in this thesis are those of the author and do not reflect the official policy or position of the Department of Defense or the U.S. Government.			
12a. DISTRIBUTION / AVAILABILITY STATEMENT Approved for public release; distribution unlimited		**12b. DISTRIBUTION CODE**	

13. ABSTRACT (maximum 200 words)

Wide bandgap semiconductors such as Zinc Selenide (ZnSe) have become popular for ultraviolet (UV) photodetectors. ZnSe has a higher photosensitivity compared to silicon-based detectors due to its larger bandgap. Its capability of turning optical power into valuable electrical signals makes it suitable for measurement and recording of UV exposure for military personnel. The prospect of ZnSe's unique medical and military applications has been the driving force of this study. This thesis presents characterization of performance of UV detectors using ZnSe-based Schottky diodes. There are a total of 15 photodetectors involved in this study. Three sets, each consisting of five photodetectors, were designed to detect Ultraviolet-A (320–400 nm), Ultraviolet-B (290–320 nm) and combination of both (UV-A and UV-B) wavelength ranges. The 15 detectors were analyzed for their photosensitivity using a photocurrent measurement system. Each diode's responsivity (ampere per watt) was determined as a function of wavelength of the incident radiation. The second part of the characterization process includes the determination of the current-voltage (IV) characteristics of the photodetectors. Each photodiode's current response was plotted as a function of both reverse and forward biased voltages and compared with the expected behavior.

14. SUBJECT TERMS Zinc Selenide, Photodetectors, Ultraviolet, Schottky, Responsivity, Current-voltage, Depletion Region, Bandgap, Melanoma, Dark Current, Forward Biased, Reverse Biased			**15. NUMBER OF PAGES** 57
			16. PRICE CODE
17. SECURITY CLASSIFICATION OF REPORT Unclassified	**18. SECURITY CLASSIFICATION OF THIS PAGE** Unclassified	**19. SECURITY CLASSIFICATION OF ABSTRACT** Unclassified	**20. LIMITATION OF ABSTRACT** UU

i

THIS PAGE INTENTIONALLY LEFT BLANK

CHARACTERIZATION OF ZINC SELENIDE-BASED ULTRAVIOLET DETECTORS

Victoriano C. Naval, Jr.
Lieutenant, United States Navy
B.S., Mapua Institute of Technology, 1988

Submitted in partial fulfillment of the
requirements for the degree of

MASTER OF SCIENCE IN APPLIED PHYSICS

from the

NAVAL POSTGRADUATE SCHOOL
December 2009

Author: Victoriano C. Naval, Jr.

Approved by: Gamani Karunasiri
        Thesis Advisor

        Craig Smith
        Second Reader

        Andres Larraza
        Chairman, Department of Physics

THIS PAGE INTENTIONALLY LEFT BLANK

ABSTRACT

Wide bandgap semiconductors such as Zinc Selenide (ZnSe) have become popular for ultraviolet (UV) photodetectors. ZnSe has a higher photosensitivity compared to silicon-based detectors due to its larger bandgap. Its capability of turning optical power into valuable electrical signals makes it suitable for measurement and recording of UV exposure for military personnel. The prospect of ZnSe's unique medical and military applications has been the driving force of this study. This thesis presents characterization of performance of UV detectors using ZnSe-based Schottky diodes. There are a total of 15 photodetectors involved in this study. Three sets, each consisting of five photodetectors, were designed to detect Ultraviolet-A (320–400 nm), Ultraviolet-B (290–320 nm) and combination of both (UV-A and UV-B) wavelength ranges. The 15 detectors were analyzed for their photosensitivity using a photocurrent measurement system. Each diode's responsivity (ampere per watt) was determined as a function of wavelength of the incident radiation. The second part of the characterization process includes the determination of the current-voltage (IV) characteristics of the photodetectors. Each photodiode's current response was plotted as a function of both reverse and forward biased voltages and compared with the expected behavior.

THIS PAGE INTENTIONALLY LEFT BLANK

TABLE OF CONTENTS

vii

THIS PAGE INTENTIONALLY LEFT BLANK

LIST OF FIGURES

LIST OF TABLES

THIS PAGE INTENTIONALLY LEFT BLANK

ACKNOWLEDGMENTS

THIS PAGE INTENTIONALLY LEFT BLANK

I. INTRODUCTION

Ultraviolet (UV) light naturally occurs and is radiated by the sun. It is classified to be located below the shorter wavelength end of the visible spectrum, which has wavelengths in the region of 400 to 700 nanometers. UV rays are invisible to the naked eye and are commonly called "bluer than blue" of the light spectrum since their wavelengths range from 100 to 400 nanometers as shown in Figure 1.
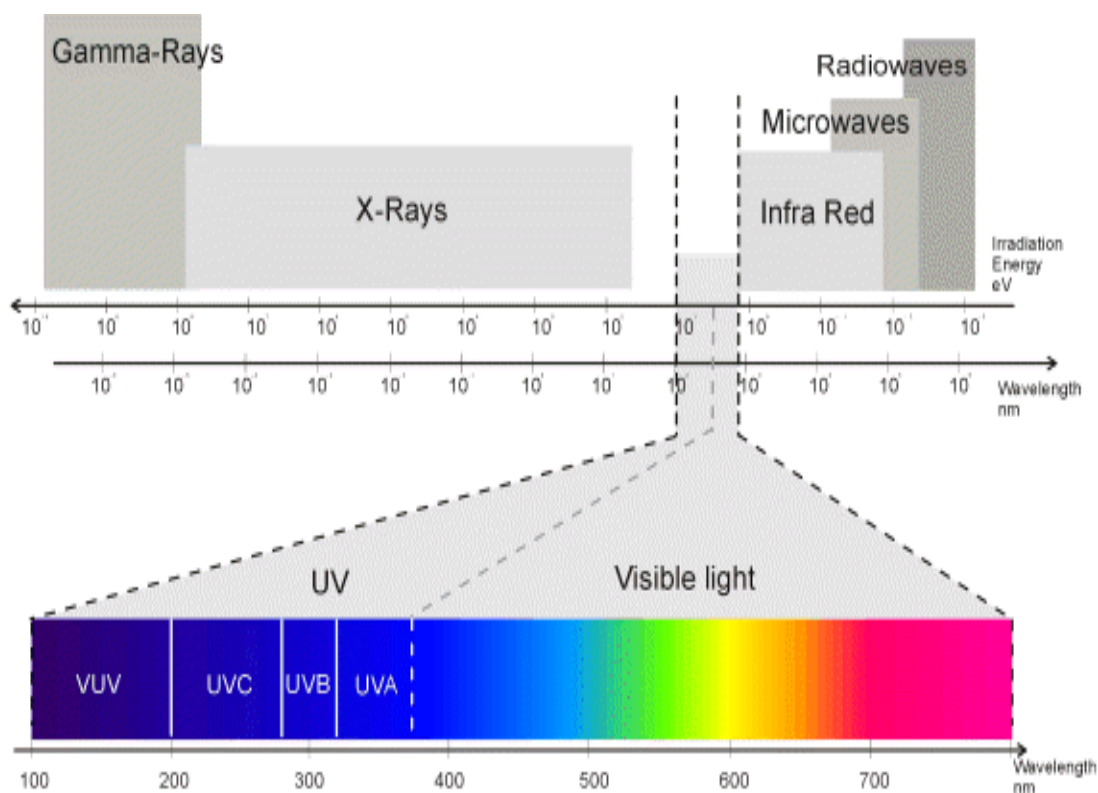
Figure 1. The UV spectrum. (From [1])

The human skin is sensitive to UV light and prolonged exposure of a dangerous level of UV radiation can produce harmful effects. Normally, the skin produces a protein called melanin, made by cells known as melanocytes, which are located in the bottom layer of skin. Melanin absorbs UV radiation in response to exposure to the sun. The

melanin protects the skin by absorbing the UV radiation and, in turn, produces a tan when the skin is exposed to sunlight. Overexposure to sunlight can lead to the malfunction and uncontrollable growth of melanocytes, resulting in skin cancer called malignant melanoma [2].

An elevated rate of military personnel contracting this type of disease prompted the Walter Reed Army Institute of Research, which is located in Bethesda, MD, to seek technical advice from Naval Postgraduate School (NPS) in identifying or developing a dosimeter suitable for monitoring UV exposure in military personnel. The practical application is to have a dosimeter system, which is capable of detecting, recording and displaying UV exposure for a minimum period of one year that can be worn as a wristband or as some other unobtrusive wearable item.

The detection of UV is typically achieved by using wide bandgap semiconductors such as gallium nitride (GaN) or zinc selenide (ZnSe) [3]. The sensors are made by forming Schottky barriers using a variety of metals such as Au or Ni. In this thesis, Schottky barrier photodiodes based on tellurium-doped zinc selenide Te:ZnSe and nickel (Ni) with integrated UV filters are characterized. Professor Craig Smith, Lawrence Livermore Chair at Naval Postgraduate School, spearheaded the requisition of both filtered and unfiltered types of the photodiodes to evaluate their performance for potential incorporation in UV dosimeters. The resulting detector samples are composed of three sets, each consisting of five of the following photodetector groups: Ultraviolet-A (320–400 nm), Ultraviolet-B (290–320 nm) and Unfiltered to include both (UV-A and UV-B) wavelength ranges manufactured by the staff of Dr. Volodymyr Ryzhikov from the Institute of Single Crystals in Kharkov, Ukraine. These photodiodes were characterized in the Sensors Research Laboratory at the Naval Postgraduate School, and are the main focus of this thesis.

A. DOSIMETER TO MONITOR ACCUMULATED UV DOSE

Numerous types of UV sensors were considered in creating a dosimeter that will detect and record UV exposure over an extended period of time, which is approximately one year. One possible type is a sensor based on the response of a photosensitive film

material [4]. In this case, the degradation of the film would be used for UV detection. Although a good sensitivity can be obtained, the photosensitive film has the disadvantages of not being reusable, and not being capable of continuously recording data over an extended period of time [4].

Other types of UV sensor were also considered, based on photoelectric response of a material [4], photoresistors or Schottky barrier structures [4].   The photoresistor has high photosensitivity; however, it could not operate in electro-generator mode. Lastly, the Schottky diode, a combination of a metal and semiconductor with a potential barrier structure, becomes the most preferred type because it has high impedance, and can operate at shorter wavelengths. Figure 2 shows a typical layout of a UV photodetector used in this thesis [4].
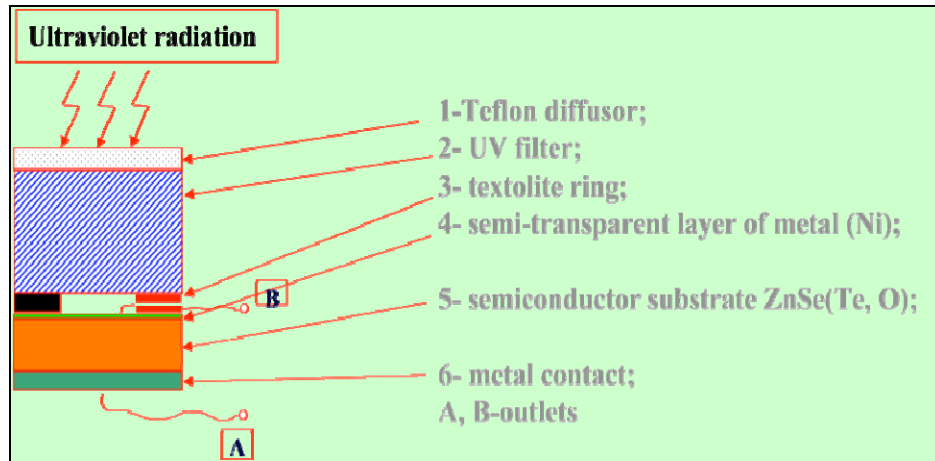
Figure 2.   Layout of a UV photodetector device. (From [4])

The Schottky diode schematically shown in Figure 2 is based on tellurium doped zinc selenide (Te:ZnSe) and nickel (Ni). It has high photosensitivity in UV spectrum and is blind to wavelengths in the visible range and higher (solar blind). Compared to other compound semiconductors, such as gallium nitride (GaN), which is also sensitive in UV region, ZnSe has a broader spectral sensitivity, as shown in Figure 3. It shows the relatively broad spectral characteristics of ZnSe-based photodiode in the UV region of 300 to 450 nm, which is needed for fabricating dosimeters in the UV A and B ranges. It was also found that the ZnSe based detectors have low leakage current compared to GaN

counterparts making them much less noisy [3]. A photograph of a typical ZnSe photodetector used in this study is shown in Figure 4.
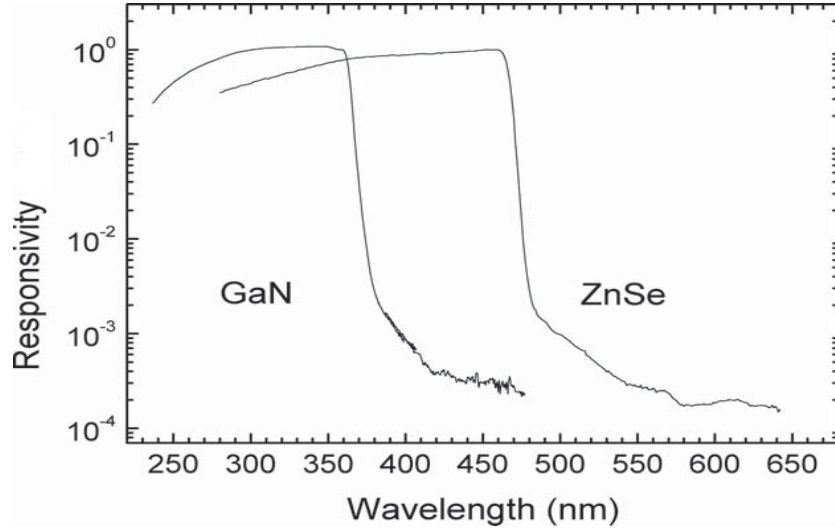
Figure 3. Normalized responsivity of GaN and ZnSe based Schottky photodiodes (From [3])
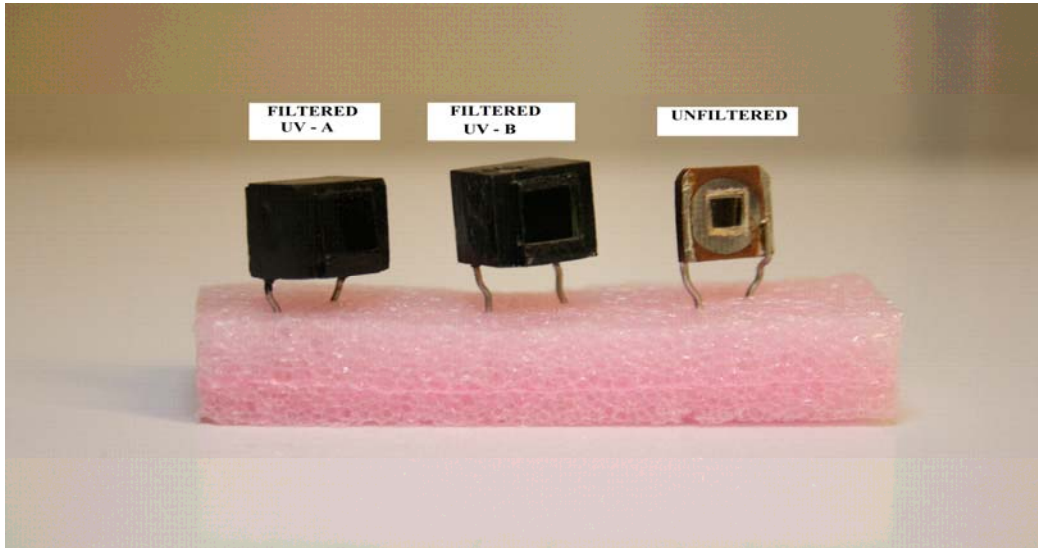
Figure 4. Packaged Ni-ZnSe Schottky photodiode

ZnSe(Te) photodiodes, based on Schottky diode and outfitted with appropriate filters, can be used as UV-A (320–400 nm) and UV-B (290–320 nm) photodiodes to measure UV dose rate. With proper integration into a system, these photodiodes will also be able to record and display readings over an extended period of time and function as a dosimeter [4].

B.   SEMICONDUCTOR DETECTORS

In semiconductors, the valence and conduction bands are separated by an energy gap commonly called bandgap energy, E_g. It is located between the top of the valence band and the bottom of the conduction band and has an average value of one electron-volt (eV). Some of the most common semiconductors' E_g are shown in Table 1.

Material	Symbol	Bandgap (eV) @ 300K
Silicon	Si	1.11
Germanium	Ge	0.67
Silicon carbide	SiC	2.86
Aluminum nitride	AlN	6.3
Diamond	C	5.5
Gallium(III) arsenide	GaAs	1.43
Gallium(III) nitride	GaN	3.4
Indium(III) arsenide	InAs	0.36
Zinc selenide	ZnSe	2.7
Zinc telluride	ZnTe	2.25
Cadmium sulfide	CdS	2.42
Cadmium selenide	CdSe	1.73

Table 1.   Bandgap energy E_g for selected semiconductors. (After [5])

The table shows that Diamond and Indium (III) Arsenide have the largest and smallest bandgap, respectively. The zinc selenide has wide bandgap energy of 2.7 eV at room temperature.

In a semiconductor, absorption occurs if the photon energy hv is greater than the bandgap energy, (i.e., $hv > E_g$). An absorption will create an electron-hole (e-h) pair as schematically shown in Figure 5. The electron absorbs the photon and gets excited to the conduction band (CB) leaving a hole, that is, the absence of an electron, in the valence band (VB). The charge carriers (electrons and holes) in the presence of an electric field move in their respective bands, thus producing photocurrent [6].
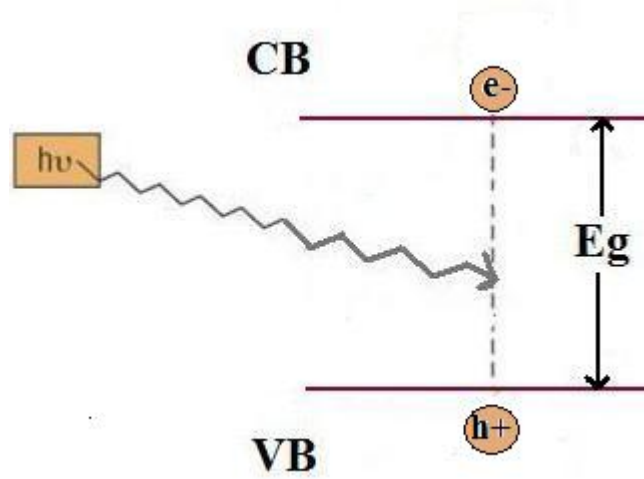
Figure 5. Electron-hole pair created from absorption of photon energy hv. (After [7])

The minimum photon energy must be at least equal to the bandgap, $hv_{min} \approx E_g$ of the semiconductor. Absorption is not possible if the photon energy is less than the bandgap, $hv < E_g$ since an electron-hole pair cannot occur and energy levels are not available for the electron in the bandgap. As the wavelength gets longer, the photon energy becomes smaller. Using $c = \lambda v$ in the condition for absorption of $hv > E_g$ gives:

$$\frac{hc}{\lambda} > E_g \implies \frac{hc}{E_g} > \lambda \tag{1.1}$$

6

and provides the subsequent equation for the maximum wavelength that can be detected by the semiconductor [6]:

$$\lambda_{max} = \frac{hc}{E_g} = \frac{1.24}{E_g} \qquad (1.2)$$

where the unit of the wavelength, λ is in μm and E_g is in electron volt (eV).

Figure 6 shows an example of photoresponse for a typical silicon p-i-n photodiode. Its effective spectral range is between 400–1100 nm. The maximum wavelength that can be detected by the photodiode is around 1.1 μm which is approximately equal to silicon bandgap energy of 1.1 eV. The graph shows that neither detection nor absorption occurs at wavelengths greater than 1.1 μm since the photon energy becomes less than the bandgap energy. On the other hand, responsivity (photocurrent per unity incident optical power) near the bandgap is strong but gradually decreases as the wavelength becomes smaller until it reaches the UV range (~400 nm). The lower responsivity at high photon energies is due to the waste of excess photon energy as heat and also strong absorption close to the surface of the diode where there is no electric field to generate photocurrent. For detection in the UV spectral range, a Schottky diode is preferred over the silicon p-i-n diode due to the formation of its junction close to the surface.
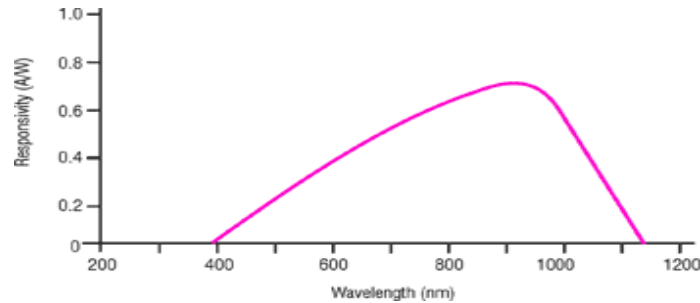
Figure 6. Responsivity as a function of wavelength for typical silicon photodiode. (From [8])

C.   SCHOTTKY PHOTODIODE

A Schottky photodiode is made of a very thin, about 100 Å, layer of metal evaporated on a doped semiconductor. If the semiconductor is n-type, the electrons from

the semiconductor will diffuse down to the metal to fill lower energy states. A brief electron flow will occur until the electric field E_o created by the flow opposes the diffusion of additional electrons [6].

Figure 7 shows the schematics of the metal and semiconductor material before and after forming the junction. Before contact, the electrons in the n-type semiconductor occupy higher energy states compared to those in the metal. After forming the junction, the energy levels of the conduction and valence bands of the semiconductor bends to allow its Fermi level E_{Fn} (dashed lines in Figure 7) to be equal with that of the metal as illustrated in Fig. 7.
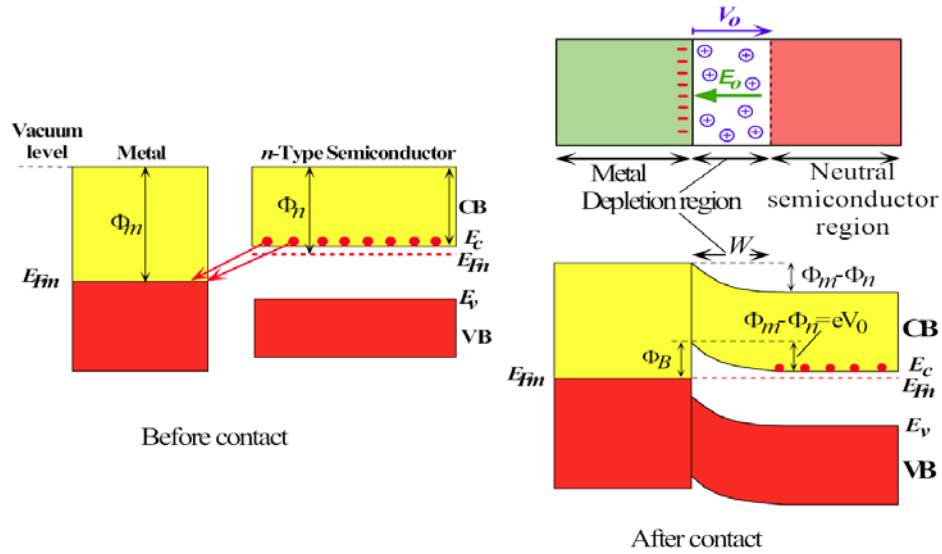
Figure 7. Formation of metal and semiconductor junction in a Schottky photodiode. Where E_{Fm} is the Fermi level of metal, the work function Φ_M is the minimum energy required to remove an electron from solid, the work function Φ_n is the minimum energy required to remove an electron from the semiconductor, Φ_B is the barrier height, V_o is the built-in potential, and E_C, E_V are the conduction and valence band edges. (From [9])

The transfer of electrons to the metal leaves behind ionized impurities in the semiconductor forming a depletion region, as well as a barrier (Φ_B), at the junction of the semiconductor and metal, as shown in Figure 7.

Schottky diodes are good photodetectors for UV rays. In comparison with other light, UV has shorter wavelengths, but a higher absorption coefficient, which is about $10^4 - 10^5 cm^{-1}$ [10]. When a UV ray is incident to a Schottky diode, absorption occurs almost at the surface, due to the very thin metal layer attached to the semiconductor, into the depletion region. It is also the region where the electric field is present. This is a big advantage of the Schottky over a p-i-n type photodiode [8].

1.   Depletion Layer Width

The calculation of the width of the depletion region can be started by using Gauss' law which gives a relationship between the electric field and the space charge density as follows:

$$\frac{dE}{dx} = \frac{\rho_{(x)}}{\varepsilon}$$
(1.3)

where $\rho_{(x)} = eN_d$ is the space charge density at position x, E is the electric field, and ε is the dielectric permittivity. N_d is the donor concentration in the semiconductor. Since the electric field, $E = 0$ at the semiconductor end of the depletion region, integration of equation 1.3 across the depletion region gives the following result:

$$E_x(x) = E_x(0) + \frac{eN_d}{\varepsilon}x$$
(1.4)

where E(0) is the electric field in the semiconductor at x = 0. Since the depletion region is within the semiconductor, the variable d will be used to define its width. Substituting these values to equation (1.4) results in:

$$E_x(0) = -\frac{eN}{\varepsilon}d$$
(1.5)

Substituting E(0) in equation 1.4, the electric field as a function of x is given by:

$$E_x(x) = -\frac{eN}{\varepsilon}[d - x]$$
(1.6)

9

Since $E = -\dfrac{dV}{dx}$, the built-in voltage can be found by integrating the area under the curve of the graph shown in Figure (8c) as
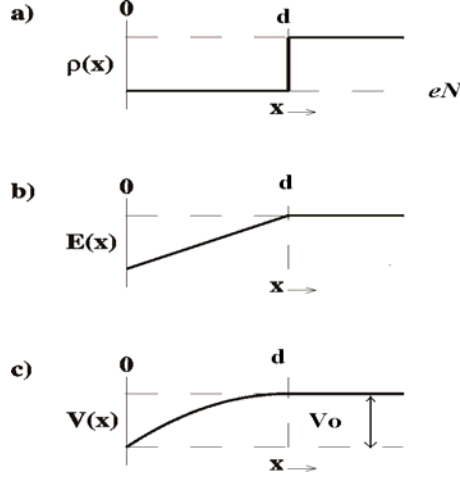
Figure 8.   Schottky barrier showing (a) space charge density (b) Electric Field and (c) Voltage [After 12]

$$V_O(x) = -\int_0^d E_x(x')dx' \qquad (1.7)$$

$$Vo = \frac{eN}{2\varepsilon}d^2 \qquad (1.8)$$

Therefore, the depletion width and built in potential are related by:

$$d = \sqrt{\frac{2\varepsilon Vo}{eN}} \qquad (1.9)$$

The longer the depletion layer width the higher the quantum efficiency of the sensor since it provides more material to capture light. The depletion width is usually controlled by adjusting the doping density in the semiconductor since $Vo \sim \Phi_b$. The cutoff wavelength of detection is determined by bandgap of the semiconductor.

D.   PROPERTIES OF ZINC SELENIDE

Zinc selenide is a light yellow binary compound from the elements Zinc (Zn) and Selenium (Se). Zinc is a transition metal, listed as the first element in Group II, which has two electrons in the outermost shell; Selenium is a nonmetal, in Group VI of the periodic

10

table, which has six electrons in the outermost shell. Combined, ZnSe normally becomes an intrinsic semiconductor with a direct bandgap of about 2.7 eV at room temperature.

Zinc selenide has the distinct property of having a high absorption coefficient at ultraviolet wavelengths and minimal absorption in the visible to near infrared region [13] as shown in Figure 9 [14].
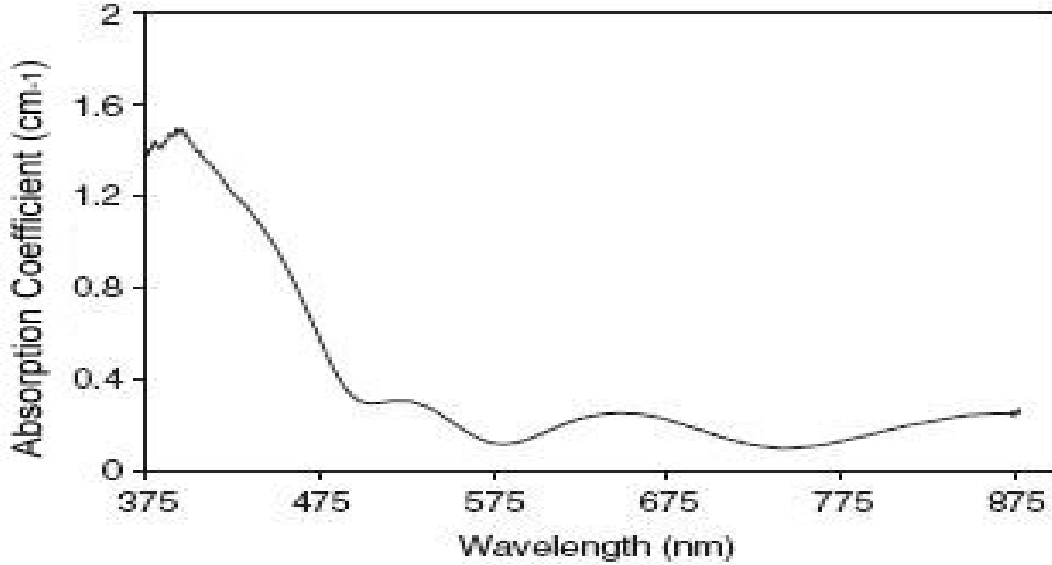
Figure 9. Absorption Spectra of Zinc Selenide in visible wavelength range. (After [14])

However, in this study, the compound was doped with tellurium, which is a p-type dopant in ZnSe, and the Schottky barrier is formed in the valence band instead of the conduction band described above. The relatively large Schottky barrier formed (~ 1 eV) generates high electric field in the depletion region, thus increasing the response speed (up to 10^{-9} s) and quantum efficiency (up to 70–80%) [15].

THIS PAGE INTENTIONALLY LEFT BLANK

II.   CURRENT VOLTAGE MEASUREMENT

The current-voltage characteristics of the ZnSe Schottky photodiodes are measured using an Agilent 4145B Semiconductor Parameter Analyzer. The equipment simply applies voltage across the detector, and then measures the corresponding current. The dark or leakage current is measured under dark condition, wherein the lid of the fixture is closed and the photodiode is not exposed to any light source. In this condition, the photodiode has high resistance. The photocurrent can be measured by exposing the sensor to light and repeating the measurement.

A.   CURRENT VOLTAGE CHARACTERISTICS

A typical current-voltage (IV) characteristic for a Schottky diode is shown in Figure 10. The graph shows the value of current as a function of voltage. At forward bias, the current rises dramatically, while a minimum leakage current occurs at reverse bias prior to the breakdown voltage. The cause of this current behavior upon application of voltages will be further analyzed in the succeeding paragraphs.
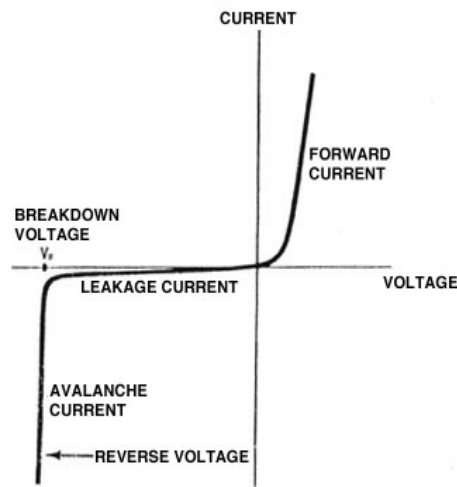
Figure 10.   Schottky diode's current-voltage characteristic in dark condition.
(From [16])

In a forward-biased diode, as shown in Figure 11a for a n-type Schottky junction, the positive terminal of the battery is connected to the metal and the negative terminal is connected to the semiconductor. The built-in electric field in the depletion region is directed towards the metal while the field due to applied voltage is directed towards the semiconductor thus reducing the built-in potential eV_o to $e(V_o - V)$, and electrons flow with less resistance towards the metal. The barrier height, Φ_B, at the junction of the metal and semiconductor remains unchanged. The sudden surge of the charged carriers to the metal make the magnitude of the current rise exponentially with bias which can be estimated using [17]:

$$I = I_o(e^{\frac{eV}{kT}} - 1) \tag{2.1}$$
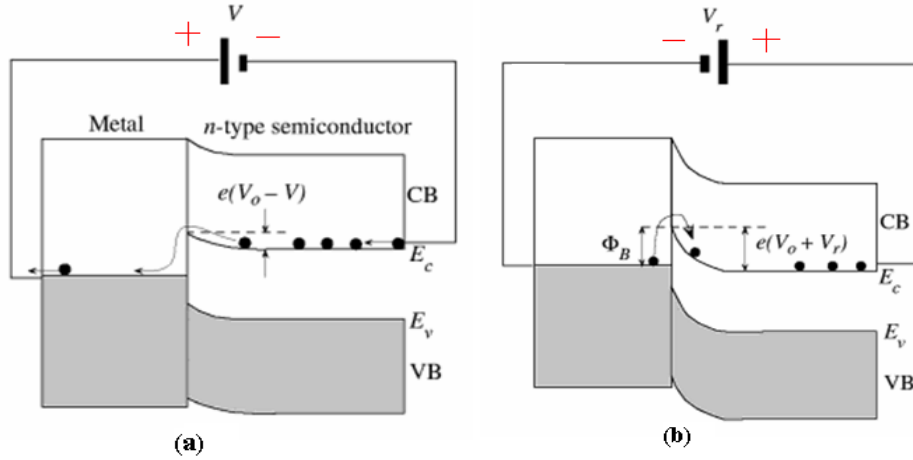
Figure 11.   Schottky junction showing (a) Forward-biased and (b) Reverse-biased conditions. (After [9])

On the other hand, the diagram of the reverse-biased Schottky junction is shown in Figure 11b. In this mode, the negative terminal is connected to the metal, while the positive terminal is connected to the semiconductor, producing a reverse voltage, $-V_r$. Both the built-in and applied fields are in the same direction, towards the metal. The sum of their voltages creates a deeper potential barrier, with energy equal to $e(V_o + V_r)$, thus making it more difficult for the electrons to travel from semiconductor to the metal. Similar to the forward-biased mode, the barrier height, Φ_B, at the junction of the metal

14

and semiconductor, remains unchanged. The limited movement of the charge carriers via thermal excitation across the Schottky barrier to the metal results in small reverse current, I_o. This phenomenon explains the tiny leakage current present in the Schottky diode at reverse-biased mode, as shown previously in Figure 10 [9]. As the reverse bias is increased, the tunneling of electrons from metal to semiconductor results in breakdown of the junction generating a large reverse current as shown in Figure 10. Operation of photodiodes near breakdown provides gain in photodetection and such detectors are commonly known as avalanche photodiodes.

B.   MEASURED CURRENT VOLTAGE DATA

The fifteen photodiodes were grouped according to the wavelength sensitivity as shown in Table 2. Their current-voltage characteristics were taken in both the dark and under light illumination.

Ultraviolet-A (320-400 nm),	Ultraviolet-B (290-320 nm)	UNFILTERED (UV-A and UV-B)
S4-41	S4-7	S4-1
S4-26	S4-14	S4-2
S4-17	S4-19	S4-3
S3-10	S4-30	S4-4
S4-18	S3-1	S4-6

Table 2.   Ultraviolet sensors grouping
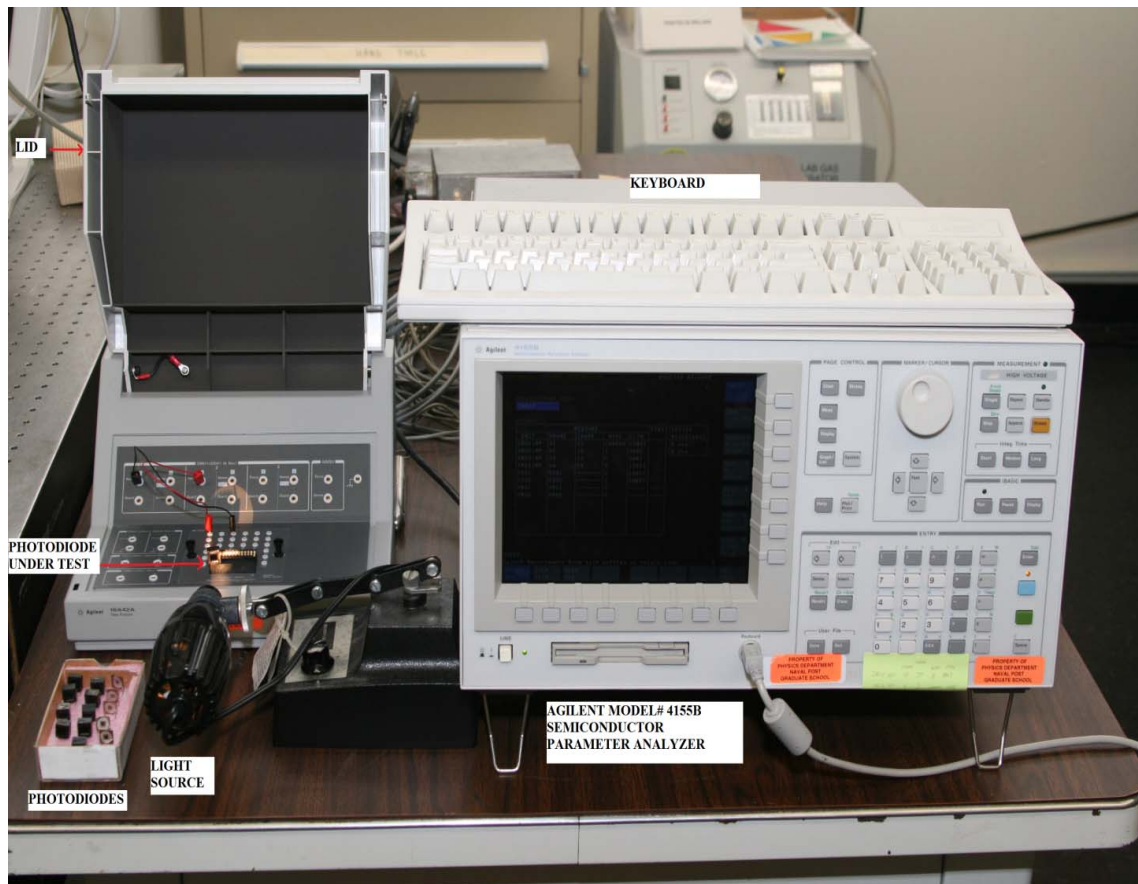
Figure 12.   Semiconductor Parameter Analyzer model 4155B

The dark condition, wherein no visible light is present, was accomplished by closing the lid of the Agilent 16442A Test Fixture machine as illustrated in Figure 12. The Semiconductor Parameter Analyzer was set at the following parameters during the measurement of the photodiodes.

Start voltage: -14 V

Stop voltage: 4 V

Number of steps: 100 at 20 mV

Current compliance: 100 mA

Graph display voltage: -14 V to 4 V

Graph display current: -400 μA to 400 μA

The number of steps signifies a current reading will be taken in every 20 mV increment while the current compliance gives the maximum current allowed to avoid damage to the photodiodes.

The measured current, under dark conditions, of the photodiodes as a function of voltage is shown in Figures 13 to 15. Each photodiode has its own distinct parameter. None of the photodiodes within the same group showed a similar characteristic. All of the photodiodes' current immediately rose exponentially in the forward direction. The reverse voltages of each photodiode clearly show different breakdown voltages.

Figure 13.   Current-voltage characteristics of UV-A photodiodes under dark condition.
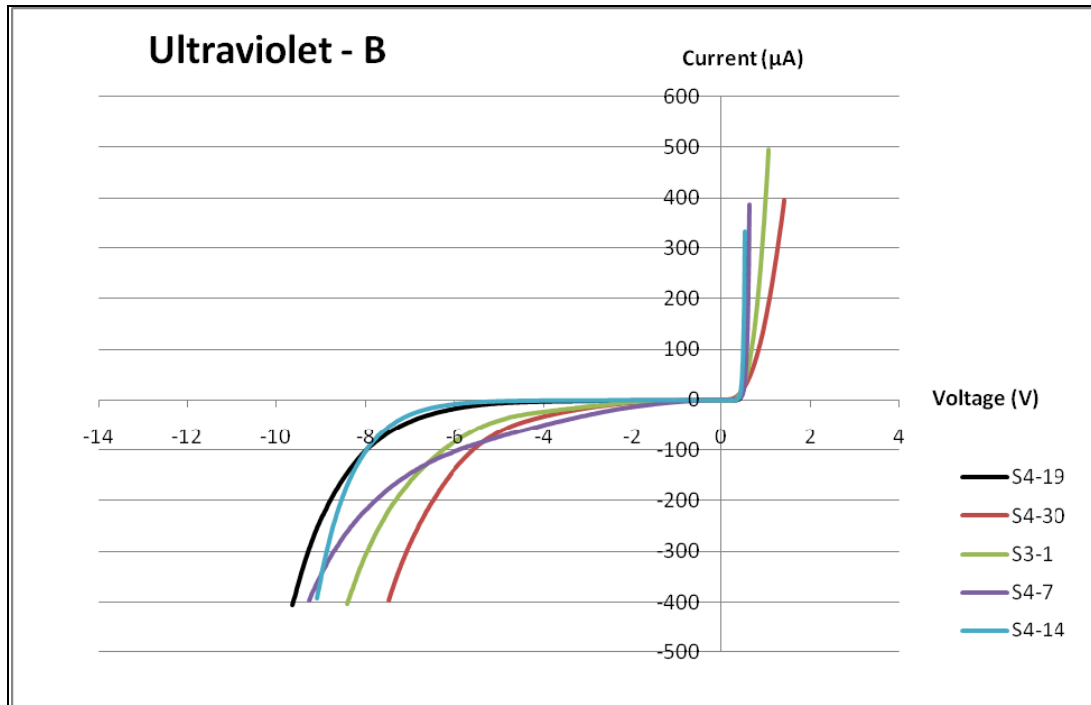
Figure 14.   Current-voltage characteristics of UV-B photodiodes under dark condition.
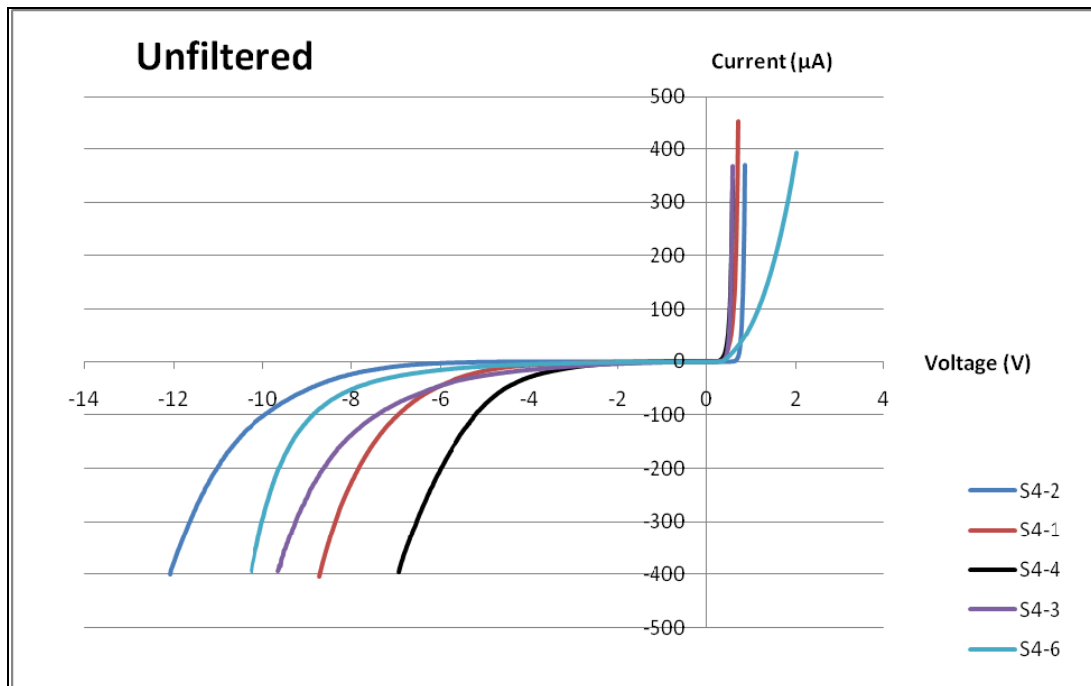
Figure 15.   Current-voltage characteristics of unfiltered photodiodes under dark condition.

18

The second part of the current-voltage measurement was performed under both dark and lighted conditions. The parameters of the Agilent 16442A Test Fixture were set at smaller current scale to measure the relatively small photocurrent along with the dark under varying light conditions using a visible light source. The resulting characteristics of the photodiodes' current as a function of voltage are shown in Figures 16 to 18.
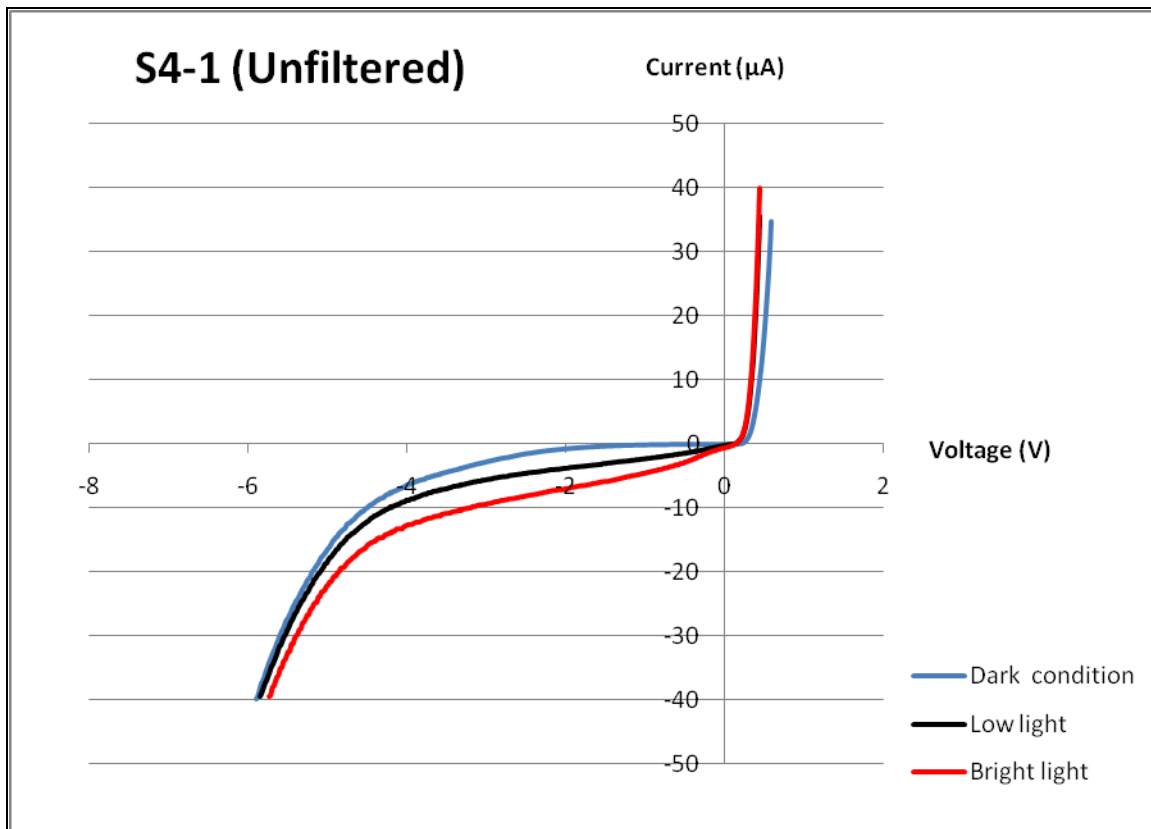
Figure 16.   Current-voltage characteristics of unfiltered photodiodes in both dark and lighted conditions.
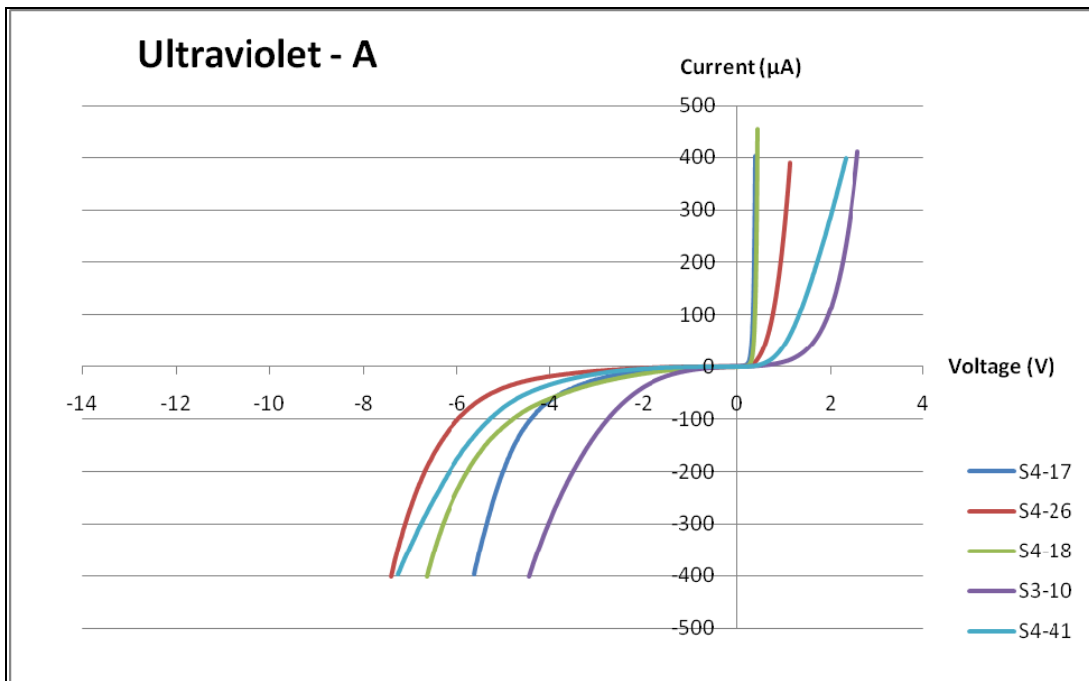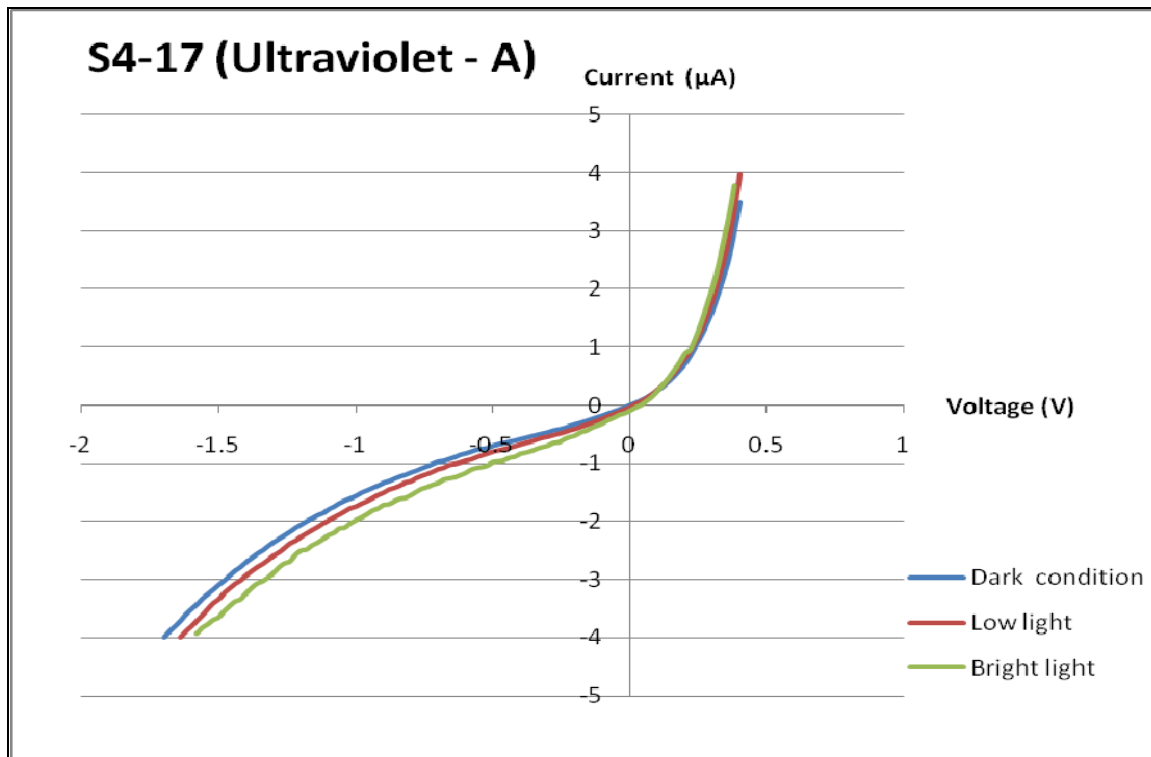
Figure 17.   Current-voltage characteristics of UV-A photodiodes in both dark and lighted conditions.
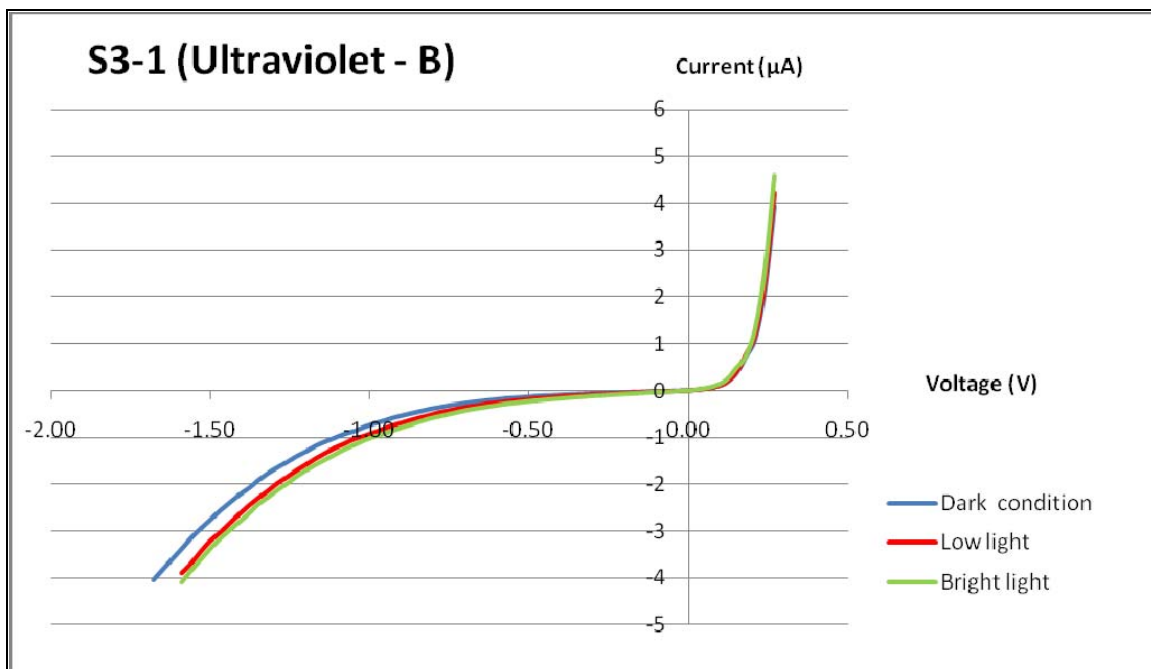
Figure 18.   Current-voltage characteristics of UV-B photodiodes in both dark and lighted conditions.

The measured data in Figures 16 to 18 shows that the reverse current increases with the intensity of the incident light due to generation of photoexcited electron-hole pairs in the semiconductor. The largest increase was observed for the unfiltered sensors (see Figure 16) since due to their broader spectral response compared to sensors with filters attached to them as shown in Figures 17 and 18. The white light source used for illumination does not produce large quantity of UV photons making the overall photocurrent relatively small.

The experimental results of the current-voltage measurements under light illumination correspond to the expected output of the photodiodes. The detailed photoresponse measurement of the sensors at different UV wavelengths will be discussed in the next chapter.

THIS PAGE INTENTIONALLY LEFT BLANK

III. SPECTRAL CHARACTERISTICS

A. OPTICAL SETUP

The second part of the characterization process of the photodiodes is the measurement of the responsivity as a function of wavelength using the photocurrent measurement equipment shown in Figure 19.
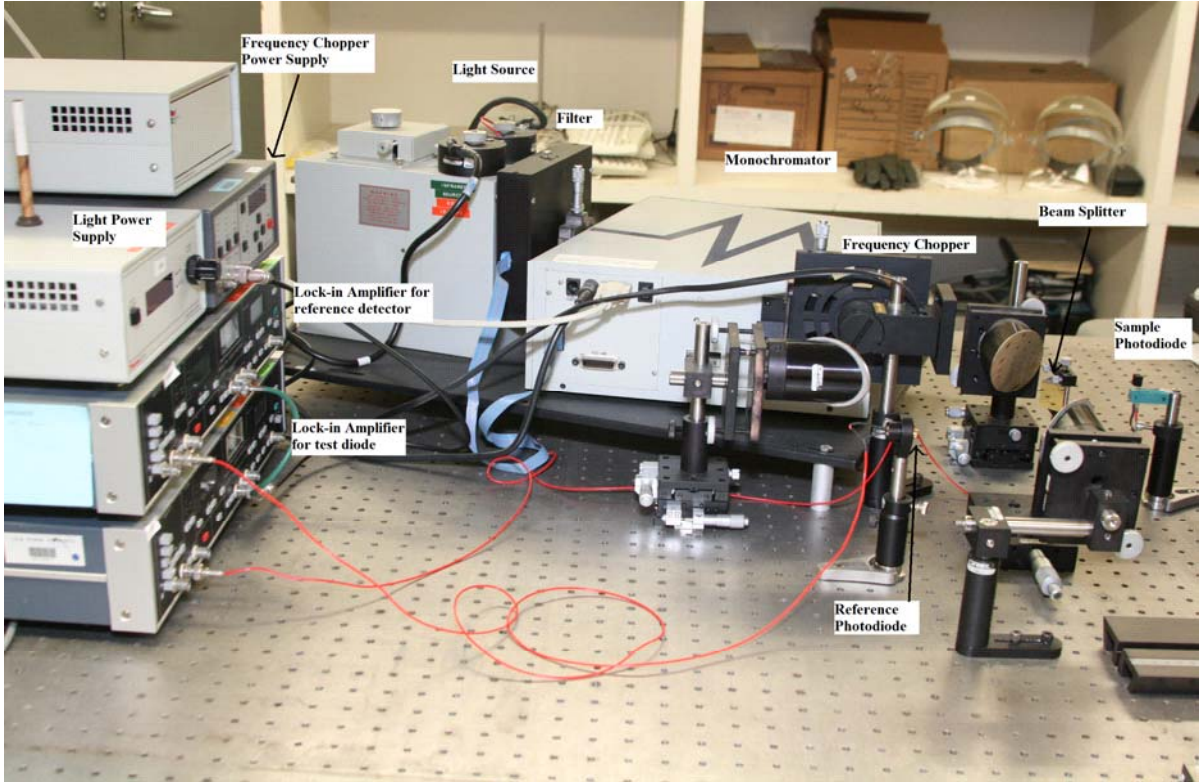
Figure 19.　　　　Laboratory setup used for measurement of responsivity as a function of wavelength.

A UV lamp is placed inside the Newport manual dual-source illuminator housing. The UV light goes through a motorized filter, which removes the higher order wavelengths. From the equation, $d \sin \theta = n\lambda$ where n is the order number, the second order wavelength with $d \sin \theta = 2\frac{\lambda}{2}$, third wavelength with $d \sin \theta = 3\frac{\lambda}{3}$, and higher order wavelengths are represented by the identical equation $d \sin \theta = \lambda$. The filter can

eliminate these higher order wavelengths preventing the second and higher order wavelengths from entering the monochromator, shown in Figure 20.
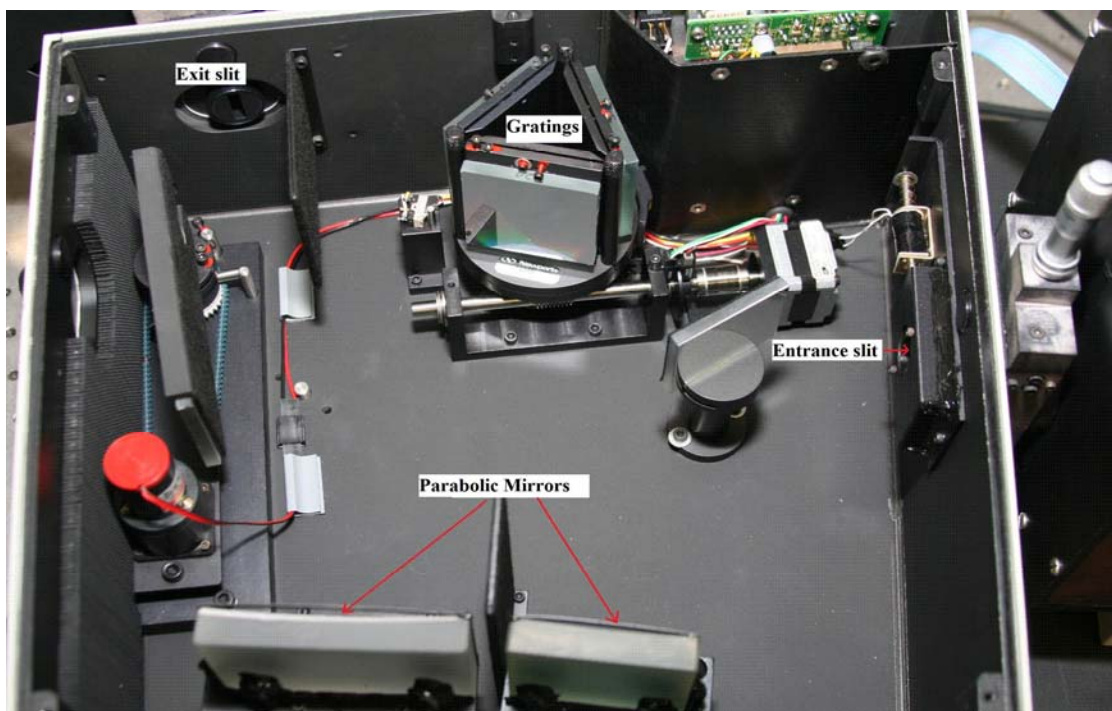
Figure 20.   Monochromator (Oriel Cornerstone 260 ¼).

The first order wavelength of UV light passes through the monochromator's entrance slit, which is set at 1.0 mm width. The UV light is reflected by a plane mirror to a parabolic mirror, which collimates the light towards the desired grating, Cornerstone 260 triple grating model# 74065, which is designed to diffract UV rays with wavelengths from 180 to 500 nm. The separated wavelengths reflect through the second parabolic mirror which, in turn, creates a parallel beam and focuses the desired wavelength to the exit slit, which has the same 1.0 mm width as the entrance slit. The wavelength resolution of the photocurrent system is about 0.5 nm.

Upon exit from the monochromator, the UV light passes through a mechanical chopper set at 140 Hz which switches the light on and off producing something similar to an alternating current (AC) signal. The chopping frequency is relayed to the lock-in amplifiers, which look for a signal from the detector at the rated frequency.

The path of the light beam after exiting the spectrometer is shown in Figure 21. The beam splits up into two equal signals at the beam splitter. Both beams travel at different directions at same path length to reach both the sample and the reference photodiodes.
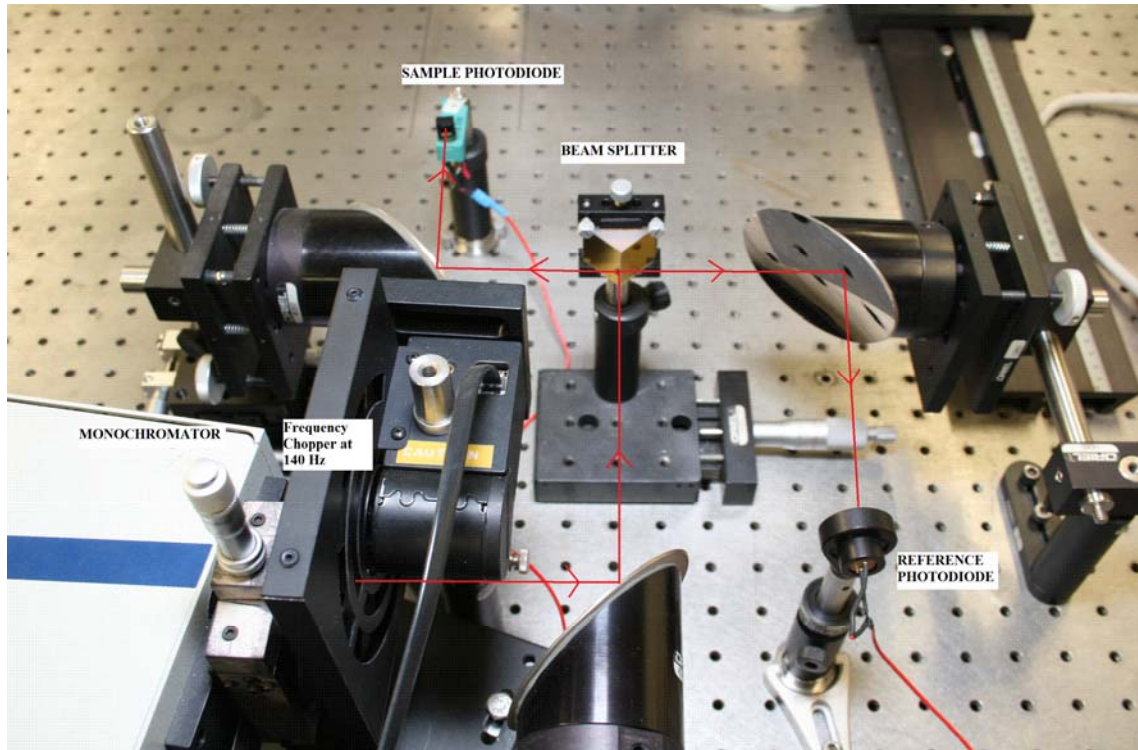
Figure 21.   Optical set-up showing the UV light travelling through the beam splitter then reflecting to both sample and reference photodiodes.

The beam on the left side of the splitter is captured by the sample photodiode while the beam on the right side of the splitter is captured by the calibrated detector acting as the reference photodiode. The signals from sample and reference photodiodes are both connected to separate lock-in amplifiers which measure the incident photocurrent produced on each respective photodiodes.

The two lock-in amplifiers are connected to a computer which uses LABVIEW software. The software graphs the photocurrents produced on both sample and reference photodiodes as a function of wavelength at certain number of steps with respect to a specified wavelength interval.

B. RESPONSIVITY

Responsivity is the ratio of the photocurrent produced to the unit power incident to the photodiode. The equation for responsivity is given by,

$$R = \frac{I}{\phi}$$ (3.1)

where I is measured in amperes and ϕ is in watts. The current can be directly measured from the lock-in amplifiers; however, the estimation of incident power requires a calibrated reference photodiode and the measurement of the area of the photodiode exposure to the incident light.

The photodiode used as a reference is a UV enhanced silicon p-i-n diode (UV-035D calibrated by UDT Sensors, INC). The graph of its responsivity as a function of wavelength is shown in Figure 22.

Figure 22. Reference silicon photodiode responsivity as a function of wavelength.

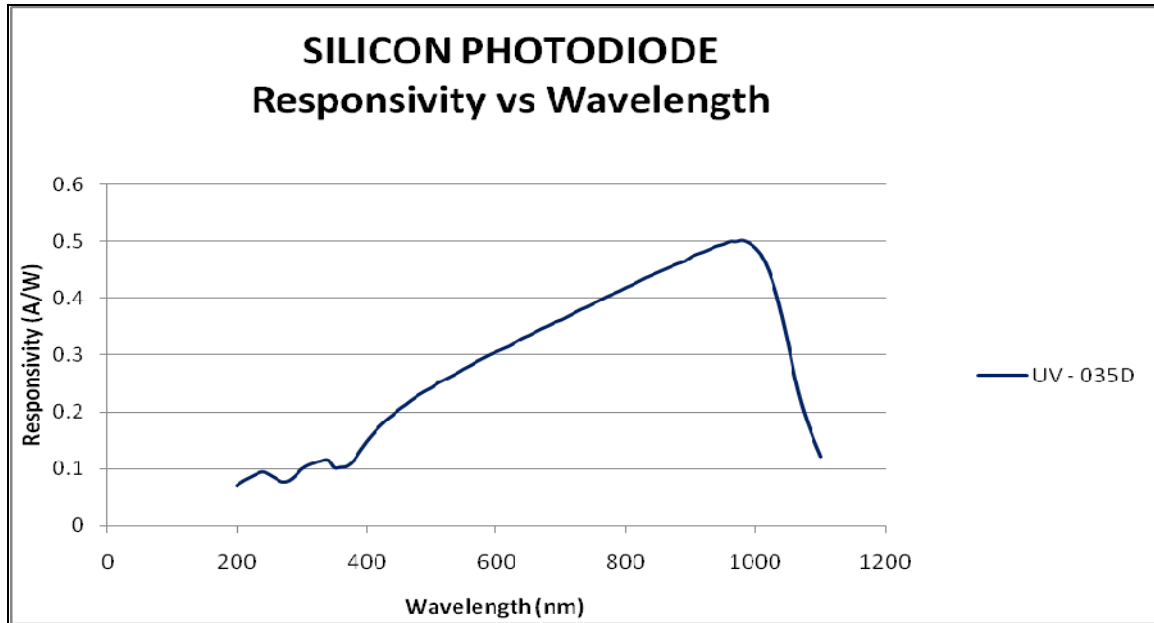The length, L and width, W of the reference's silicon photodiode are both 5.8 mm while the length and width of the sample photodiodes are both 3 mm. Since the slit width of the output of the spectrometer is 1 mm, the effective area exposed to UV radiation is 1 mm x 5.8 mm and 1 mm x 3 mm for the reference and sample photodiodes,

respectively. Since the intensity of light at each detector is the same, the power received by the sample (ϕ_S) and reference (ϕ_R) are related by

$$\frac{\phi_S}{L_S \, W_S} = \frac{\phi_R}{L_R \, W_R} \tag{3.2}$$

where L and W are the height and width of the light beam seen projected on sample (S) and reference (R). The width dimension in the equation cancels out since it is the same (1 mm) for both the sample and reference. Thus, the incident power on the sample is given by:

$$\phi_S = \phi_R \, \frac{L_S}{L_R} \tag{3.3}$$

Using equation 3.1, the incident power on the sample can be determined using the measured photocurrent of reference detector as

$$\phi_S = \frac{I_R \, L_S}{R_R \, L_R} \tag{3.4}$$

The equation for responsivity for the sample is

$$R_S = \frac{I_S}{\phi_S} \tag{3.5}$$

Substituting equation 3.4 into equation 3.5 gives,

$$R_S = \frac{I_S \, R_R \, L_R}{I_R \, L_S} \, . \tag{3.6}$$

The heights of the illuminated area for the reference and the sample are 5.8 mm and 3 mm, respectively. The reference detector responsivity, R_R, given in Figure 22 can be used for determining the responsivity of the sample.

27

C.   RESPONSIVITY MEASUREMENT

The spectral characterization process of the photodiodes started with the measurement of the photocurrent as a function of wavelength. Table 3 shows the settings used for the LABVIEW program and lock-in amplifiers. These values were adjusted to suit each of the photodiode's wavelength sensitivity.

PHOTODIODE	WAVELENGTH RANGE	WAVELENGTH INTERVAL	SAMPLE SCALE	SAMPLE MAGNIFICATION	REFERENCE SCALE	REFERENCE MAGNIFICATION
UV – A	290 – 430 nm	3 nm	30 mV	10^6	3 mV	10^6
UV – B	250 – 350 nm	3 nm	100 μV	10^6	3 mV	10^6
UNFILTERED	250 – 500 nm	3 nm	100 mV	10^6	3 mV	10^6

Table 3.   LABVIEW and lock-in amplifiers settings used for spectral characterization.

The measured photocurrents as a function of wavelength for each of the photodiodes are shown in Figures 23–25. Similar to the first part of the characterization process for current-voltage measurements, photodiodes were grouped according to their respective spectral sensitivities for comparison. The photodiodes exhibited different amount of photocurrent and none shared a common response in terms of amplitude, though the response shapes were similar. In the UV-A range, photodiode S4-26 produced the most photocurrent with a peak of 1.14 nA at 368 nm. In UV-B range, photodiode S4-7 had the highest photocurrent of 0.116 nA at 322 nm and finally the unfiltered photodiode S4-2 had 16.03 nA at 455 nm.
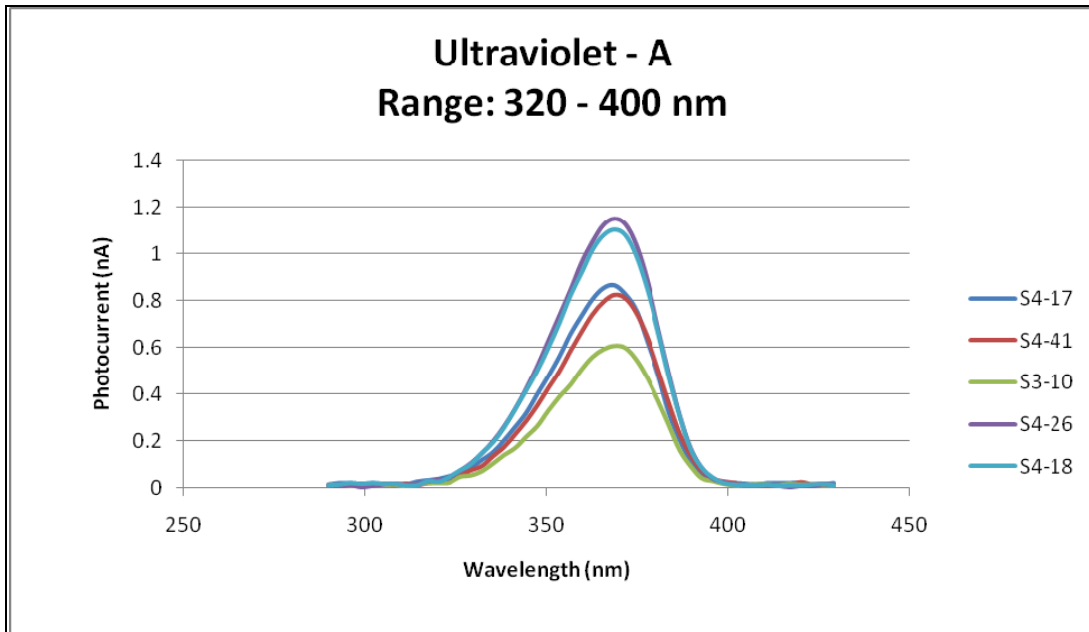
Figure 23.   Measured photocurrent as a function of wavelength for UV-A photodiodes.
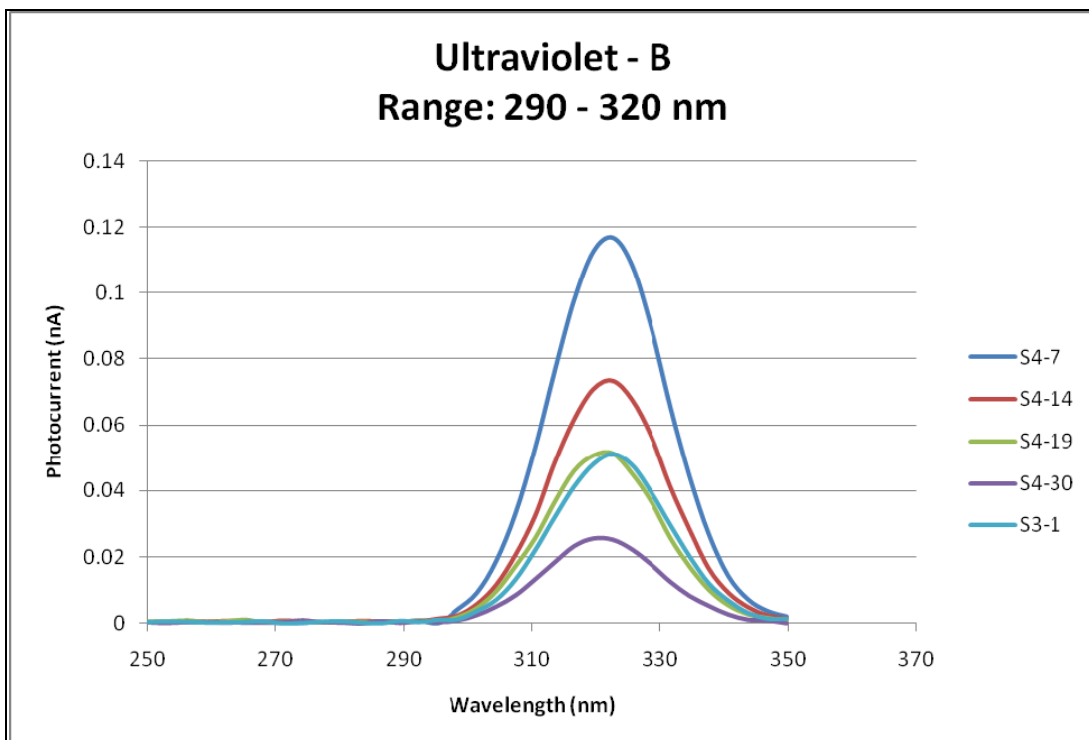

Figure 24.   Measured photocurrent as a function of wavelength for UV-B photodiode.
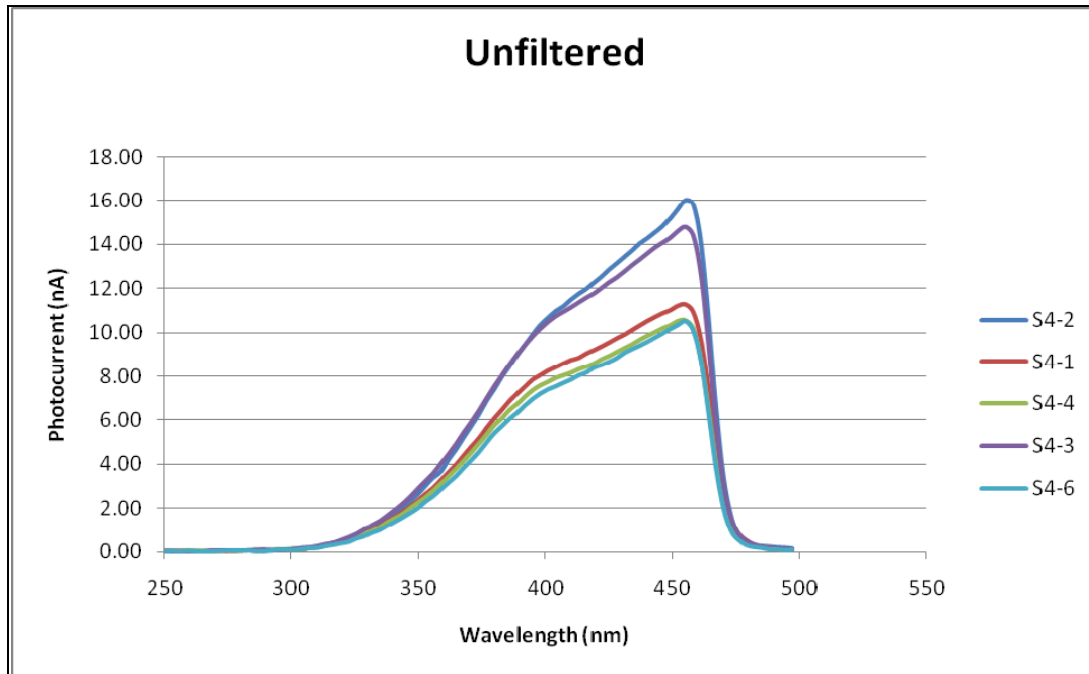
Figure 25.　　　　Measured photocurrent as a function of wavelength for unfiltered photodiodes.

It can be seen from Figures 23–25 that the unfiltered photodiodes produced the highest photocurrent since they are receiving the full optical power from the incident light. The filtered sensor's actual power received depends on the transmittance of the filters which are not known at present.

The spectral responsivities of the photodiodes were estimated using the measured photocurrents and equation 3.6 and are shown in Figures 26–29. Similar to the measured photocurrents, each photodiodes has its own distinctive responsivity. Two photodiodes with the highest responsivity were selected from UV-A and UV-B group and plotted in Figure 28. It can be seen that the photodiode S4-26 from UV-A had a peak responsivity of 0.05 A/W compared to the photodiode S4-7 from UV-B with a much lower responsivity of 0.01 A/W.

Similar to the photocurrent characteristics, the unfiltered photodiodes exhibited the largest responsivity. It was expected since the unfiltered photodiode receives larger power on the surface of it compared to the filtered sensors. The higher the value for the

30

photocurrent, the larger the resulting responsivity. The measured values of responsivity for unfiltered photodiodes are in good agreement with previously reported values for similar Schottky diodes [18].
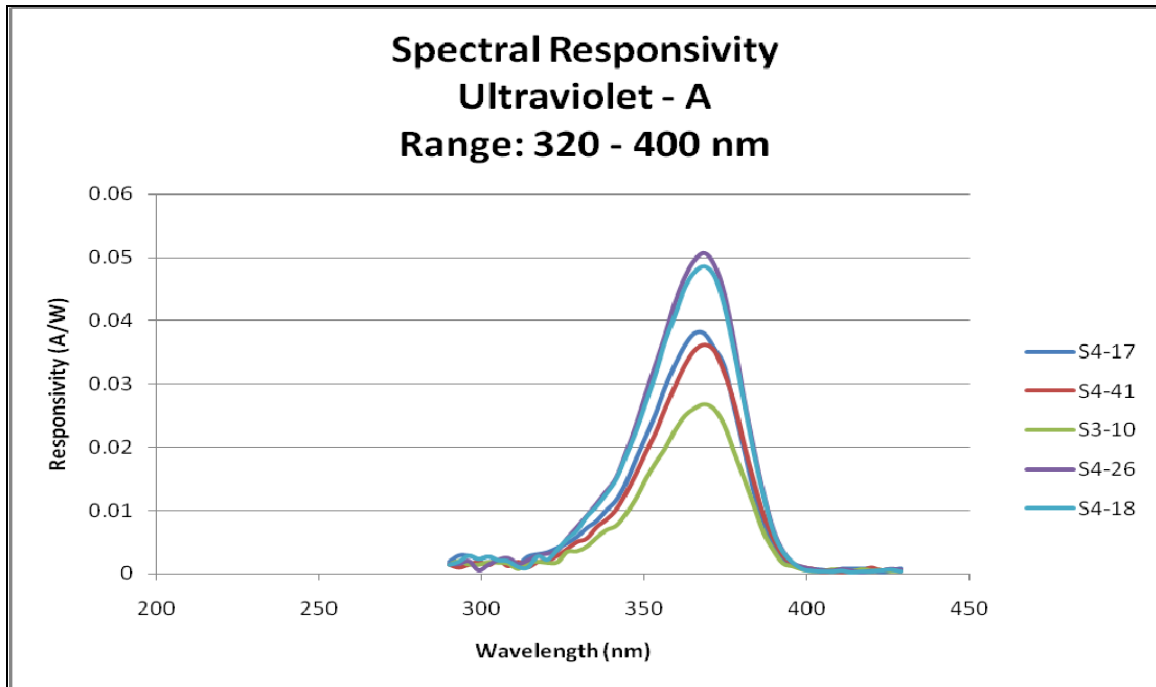

Figure 26.   Spectral Responsivity as a function of wavelength for UV-A photodiodes.
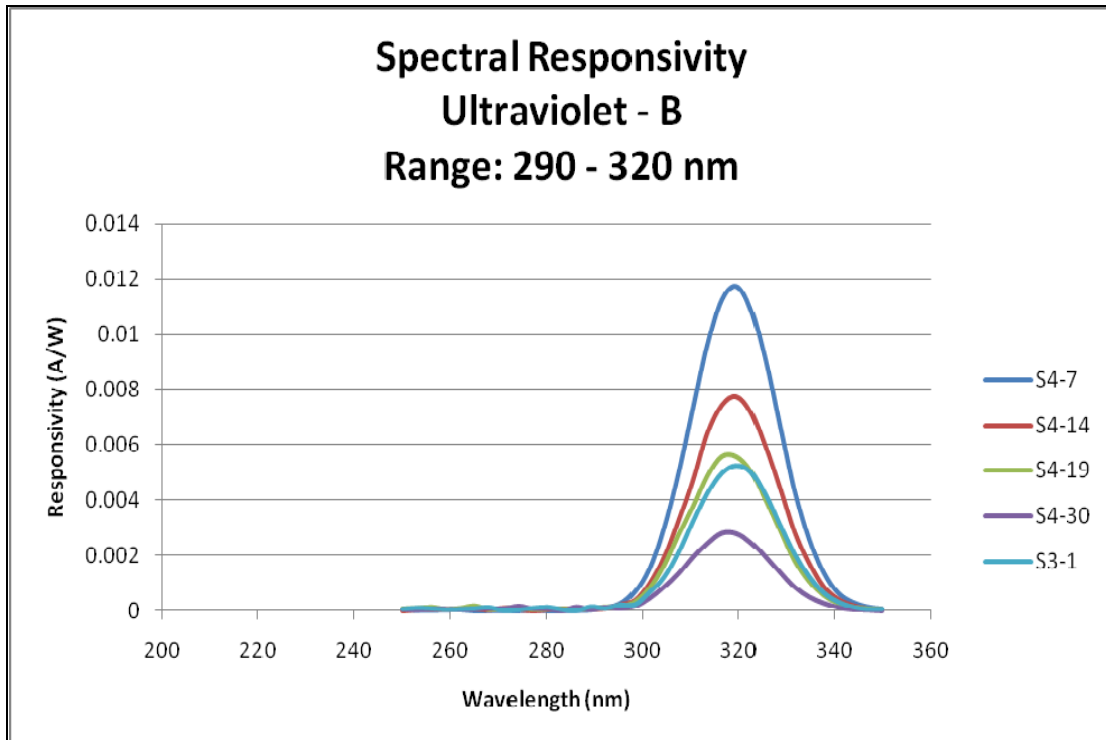
Figure 27.   Spectral Responsivity as a function of wavelength for UV-B photodiodes.
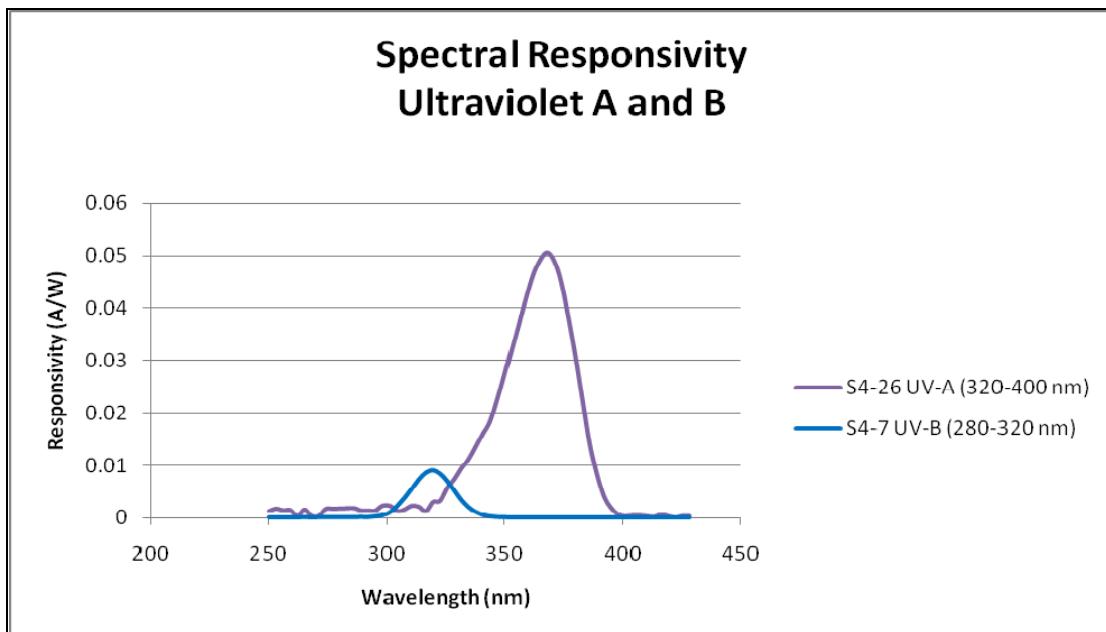
Figure 28.   Comparison of the two sensors with highest spectral responsivity from both UV-A and UV-B photodiodes.
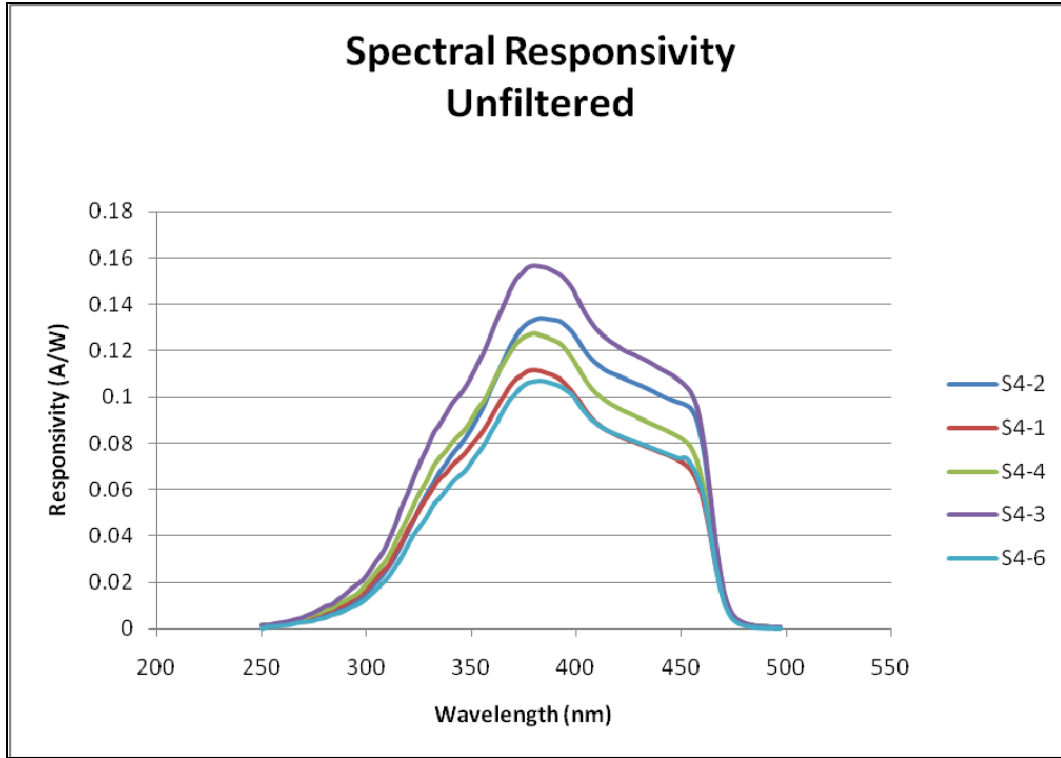
Figure 29.   Spectral Responsivity as a function of wavelength for unfiltered photodiodes.

D.   CUTOFF WAVELENGTH AND BANDGAP

Figure 29 shows a broader spectral responsivity spectrum for the unfiltered photodiodes compared to the results for UV-A and UV-B ranges. A sudden decrease in responsivity was measured at around 458 nm. At this point, the photon energy reached the bandgap. Any photon with a wavelength greater than 458 nm has less energy than the amount necessary for absorption and will pass through the photodiode. Using the above cutoff wavelength, the corresponding photon energy can be estimated using

$$hv = \frac{1.24}{\lambda} \, (eV) \qquad\qquad (3.7)$$

where the wavelength , λ is in μm. The estimated bandgap of the ZnSe is about 2.7 eV.

In addition, the type of band gap of ZnSe can be determined from the experimental results of Figure 29 near the cutoff. The amount of the photocurrent produced during absorption of a photon depends on the excess energy produced from the

33

difference of the photon energy hv and the bandgap energy, E_g. Near the bandgap edge of the semiconductor, the proportionality of the photocurrent in relation to the excess energy determines the type of the bandgap as shown in the following equations:

Direct Bandgap:

$$I \ \alpha \ (hv - E_g)^{\frac{1}{2}} \tag{3.8}$$

$$I^2 \ \alpha \ (hv - E_g) \tag{3.9}$$

Indirect Bandgap:

$$I \ \alpha \ (hv - E_g)^2 \tag{3.10}$$

$$\sqrt{I} \ \alpha \ (hv - E_g) \tag{3.11}$$

Plotting the values of the photocurrent near the cutoff of 458 nm as a function of the photon energy in relation to equations 3.9 and 3.11 it is possible to determine the type of ZnSe bandgap. Figure 30 shows the plot based on equation 3.9 giving a linear relationship indicating the direct nature of the bandgap. The intercept of the line at x-axis gives the bandgap of ZnSe and found to be about 2.64 eV. This value agrees well with the reported value of 2.7 eV [5].
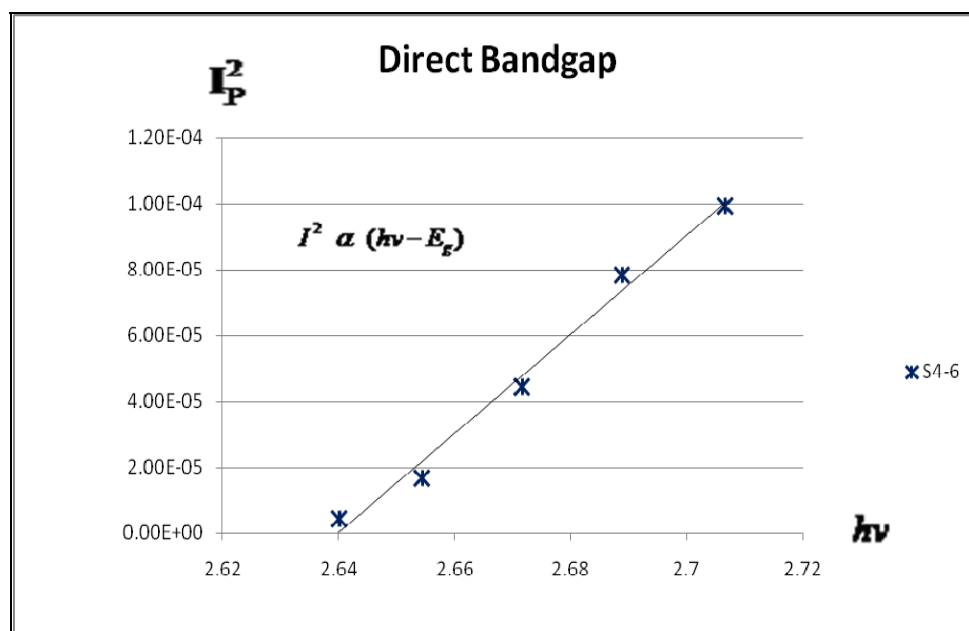
Figure 30.   Plot of square of photo current versus photo energy near the band edge. The x-intercept is 2.64 eV showing agreement with the reported value of 2.7 eV.

THIS PAGE INTENTIONALLY LEFT BLANK

IV.   CONCLUSION

The electrical and optical properties of a set of Te:ZnSe/Ni Schottky barrier photodiodes were studied experimentally.   The study included three different types (unfiltered, and with filters to detect either UVA or UVB).

The I-V characteristics clearly showed the expected diode-like behavior.   The measured I-V under light illumination showed the increase in reverse current due to generation of photocurrent in the diodes.   As expected, unfiltered diodes showed the largest photocurrent since the filters reduce the amount of light entering the sensors.

Spectral responses of the photodiodes were probed using photocurrent spectroscopy.   The unfiltered sensors show broad response in UV spectral range.   The filtered detectors clearly showed detection either in UVA or UVB ranges with good discrimination.   None of the detectors show any response in the visible spectral range due to large bandgap of ZnSe.   The responsivities of all 15 detectors were estimated using the measured photocurrent and UV power using a calibrated silicon p-i-n photodiode. Maximum responsivity of 0.11 A/W was obtained for unfiltered sensors which are comparable to reported values for similar detectors.

In addition to responsivity, the bandgap and material type of the sensors was determined using the responsivity data near the band edge. The data showed that ZnSe is direct bandgap material with bandgap energy of 2.64eV.   These findings are in good agreement with published data.   Without a doubt, the filtered and unfiltered photodiodes tested are ready to perform their designed purpose to detect UV radiation.   Further work in integration with electronics, these photodiodes will become perfectly suitable for application as dosimeter to detect, measure, record and display UV exposure of military personnel for an extended period of time. Hopefully, the medical benefits, in addition to the potential prevention of skin cancer, of this study will expand significantly and great success can be anticipated in the intended applications to save precious life.

THIS PAGE INTENTIONALLY LEFT BLANK

LIST OF REFERENCES

[1] *ZONTEC Ozone Generators*, http://www.zontecozone.com/faqs/#q6, Website last accessed 19 November 2009.

[2] Craig Smith, Private discussion, Thesis Co-Advisor, Naval Postgraduate School, Monterey, CA, July 2009.

[3] M. Hanzaz, A. Douhdada, F. Vigue, and J.P. Faurie, *ZnSe-and GaN-based Schottky Barrier Photodetectors for Blue and Ultraviolet Detection,* Philadelphia, PA: Old City Publishing Co., 2007

[4] Craig Smith, *Concept Description: Dosimeter to Monitor Accumulated UV Dose,* Point paper, Naval Postgraduate School, Monterey, CA. July 2009.

[5] *Band Gap*, http://en.wikipedia.org/wiki/Band_gap, Website last accessed 17 August 2009.

[6] R. Quimby, *Photonics and Lasers: An Introduction*, Hoboken, NJ: Wiley-Interscience, 2006.

[7] *Solid State Technology*, http://www.solid-state.com/display_article/313364/5/none/none/Dept/Technology-news, Website last accessed 17 August 2009.

[8] "Type of Detectors," http://cord.org/step_online/st1-6/st16eii1.htm, Website last accessed 5 October 2009.

[9] S. O. Kasap, *Principles of Electronic Materials and Devices Third Edition*, New York: McGraw-Hill, 2006.

[10] Gamani Karunasiri, Personal interview, Thesis Advisor, Naval Postgraduate School, Monterey, CA, August 2009.

[11] John Allison, *Electronic Engineering Semiconductors and devices,* Maidenhead, Berkshire, England: McGraw-Hill Book Company, 1971.

[12] *Theory of Electrical Characterization of (organic) Semiconductors*, by Peter Stallinga http://ceot.ualg.pt/OptoEl/theory/2terminal/, Website last accessed 14 September 2009.

[13] *Shanghai Dream Lasers Technology*, http://www.dreamlasers.com/products/crystal/znse.htm, Website last accessed 3 October 2009

[14]   Dinesh Patidar, Kuldeep S. Rathore, N.S. Saxena, Kananbala Sharma and T.P. Sharma, "Determination of optical and electrical properties of ZnSe thin films," *Journal of Modern Optics*, October 2008.

[15]   Craig Smith, *Ultraviolet solar sensors on the base of zinc selenide for climate change monitoring and environmental control*, Point paper, Naval Postgraduate School, Monterey, CA, September 2009.

[16]   *"Solar Cells,"* http://org.ntnu.no/solarcells/pages/Chap5.php, Website last accessed 8 October 2009.

[17]   Gamani Karunasiri, Personal interview, Thesis Advisor, Naval Postgraduate School, Monterey, CA, October 2009.

[18]   Amanda D. Francoeur, **"**Radios Broadcast into the Ultraviolet," http://www.photonics.com/Content/ReadArticle.aspx?ArticleID=39191, last accessed 17 November 2009.

INITIAL DISTRIBUTION LIST

1.   Defense Technical Information Center
     Ft. Belvoir, Virginia

2.   Dudley Knox Library
     Naval Postgraduate School
     Monterey, California

3.   Gamani Karunasiri
     Naval Postgraduate School
     Monterey, California

4.   Craig Smith
     Naval Postgraduate School
     Monterey, California

5.   Victoriano Naval
     SSC Pacific
     Yokosuka, Japan